JOURNAL OF THERMOPHYSICS AND HEAT TRANSFER
Vol. 15, No. 3, July–September 2001

Visualization of Flow Boiling in an Annular Heat Exchanger Under Microgravity Conditions

D. T. Westheimer*
Texas A&M University, College Station, Texas 77843
and
G. P. "Bud" Peterson†
Rensselaer Polytechnic Institute, Troy, New York, 12180-3590

An experiment consisting of a glass annular heat exchanger was flown on NASA's KC-135 reduced gravity aircraft to study the effects of gravity on flow boiling. Visual data were taken to determine flow boiling regimes, which were then analyzed using five different flow regime maps. The flow regime maps enabled predictions of the quality, two-phase heat-transfer coefficients and wall temperatures in the axial direction during periods of reduced gravity. Results from this work illustrated the following trends: 1) less heat addition was needed to cause flow regime transitions in reduced gravity environments; 2) Earth-based flow regime maps did not correlate well with visual data or zero-*g* flow regime maps; 3) all of the zero-*g* flow regime maps produced similar results for calculations of quality, heat-transfer coefficient, and heat-exchanger temperature, indicating that all of them were acceptable for this application; and 4) that maximum heat transfer occurred at locations in the heat exchanger near the transition from bubble to slug flow.

Nomenclature

A	=	cross-sectional area, m^2
D	=	tube diameter, m
m	=	mass flow rate, kg/s
S	=	slip coefficient, U_G/U_L
U	=	velocity, m/s; void fraction, A_G/A_{TOTAL}
U_{GS}	=	superficial vapor velocity, $xm_{\text{TOTAL}}/({}_G A_{\text{TOTAL}})$, m/s
U_{LS}	=	superficial liquid velocity, $(1-x)m_{\text{TOTAL}}/({}_L A_{\text{TOTAL}})$, m/s
x	=	thermodynamic quality, m_G/m_{TOTAL}; density, kg/m^3; surface tension, N/m; viscosity, N s/m^2

Subscripts

L	=	liquid phase
G	=	gas or vapor phase

Introduction

TWO-PHASE thermal systems have excellent potential in space applications because the heat-transfer capacity associated with phase change is typically large. Increased heat-transfer capabilities could mean decreased size and weight of a thermal system. These characteristics make two-phase systems extremely desirable for space applications. Because gravity greatly affects the fluid dynamics of the boiling process, possibly leading to unpredictable performance of a two-phase thermal system, it is necessary to conduct experiments and create new analytical models for reduced gravity conditions.

To explore the effects of gravity on two-phase thermal systems, a vertically oriented, annular heat exchanger was constructed of glass and flown on NASA's KC-135 reduced gravity aircraft. Refrigerant-113 was selected as the test fluid and was boiled while flowing through the center tube of the heat exchanger. As the airplane flew parabolic trajectories, the effective gravitational acceleration varied from 1.8 *g* during nose-up and nose-down maneuvers to approximately 0 *g* at the top of each parabola. Each period of reduced gravity lasted about 25 s, and over 200 parabolas were flown during the one-week test period. Visual observations during these flights confirmed that changing gravitational acceleration strongly affected the fluid dynamics of the boiling liquid.

In addition to their qualitative value, a quantitative assessment was made using the visual observations in combination with flow regime maps. Special reduced gravity models were used to analyze the experimental data, and the results were compared with a model based on Earth's normal gravity. This data reduction also enabled predictions of local heat-transfer coefficients and wall temperatures axially along the heat exchanger. Finally the uncertainties in these heat-transfer coefficients and wall temperatures caused by the flow regime map used were examined.

Experimental Apparatus and Analysis

Experimental Apparatus

The focal point of the experiment was a glass annular heat exchanger shown in Fig. 1. Borosilicate glass tubes allowed visual observations of the R-113 boiling in the center tube. The heat exchanger was 58.4 cm long, and the inner and outer diameters of the tubes were 10, 12, 65, and 70 mm, respectively. Water flowed downward with respect to gravity through the outer annulus and heated the R-113, which was flowing upwards in the center tube.

Volumetric flow rates and inlet and exit temperatures were measured for both fluids. Inlet and exit pressures of the R-113 were also measured to determine saturation conditions. Uncertainties for these measurements are shown in Table 1.

Data were recorded at a frequency of 2 Hz using a laptop computer. Visual data were recorded using a Hi8 video camera and a linear scale attached to the test apparatus to determine axial position.

The test facility consisted of two separate fluid systems that delivered water and R-113 to the annular heat exchanger at prescribed conditions. Figure 2 shows a schematic of these systems. Major components include gear pumps, piston-cylinder accumulators, and electric cartridge heaters in both loops. In addition, the R-113 loop also contained a condenser to prevent vapor from entering the pump and a needle valve to reduce the system pressure directly before the test section. The test matrix consisted of the five combinations of heater input voltages shown in Table 2.

System pressures were maintained at a value near atmospheric pressure, and fluid flow rates for all data points were approximately 100 mL/min and 24 mL/s for R-113 and water, respectively. The data

Received 3 February 2001; revision received 12 March 2001; accepted for publication 16 March 2001.

*Research Assistant, Department of Mechanical Engineering.
†Provost, Mechanical Engineering, Aeronautical Engineering, and Mechanics Department. Fellow AIAA.

taken during the week of flying on the KC-135 were then reduced using the following procedures.

Data Selection

The ever-changing environment on the KC-135 led to fluctuations in the performance of the experimental system. Westheimer[1] discussed fluctuations in system parameters, their periodic nature, and how they related to the parabolic flight of the aircraft. Because system conditions were often transient, careful data evaluation was essential to meaningful analysis. The following procedure was used to reduce fluctuations in the data and define the steady-state test conditions.

First, all measured values were averaged for periods where the acceleration as a result of gravity was 0.0 $g \pm 0.1$. Next, data points were removed from the beginning and end of the reduced gravity period until the standard deviation of the R-113 volumetric flow rate was either less than 2.00 mL/min, or decreased by less than 10% when three consecutive data points were removed. Any parabolas that did not meet the following criteria were then discarded: 1) standard deviation of the R-113 volumetric flow rate was less than 10% of the averaged value; 2) standard deviation of the inlet R-113 temperature was less than 1% of the averaged value in °C; 3) standard deviation of the inlet R-113 pressure was less than 4.89 kPa; and 4) standard deviation of the inlet water temperature was less than 0.2°C

These data selection criteria were based on those used by Reinarts et al.[2] for a similar experiment. In addition to the quantitative data taken, visual observations of the flow regime transitions and the axial location were made during each parabola. All of these data were then averaged for each test condition producing five data sets. The following analysis was performed on these five data sets.

Table 1 Experimental uncertainties

Parameter	Uncertainty	Percent of measured value
Flow rate, water	±2.2 mL/s	9
Flow rate, R-113	±2 mL/min	2
Temperatures	±0.5°C	——
Pressures	±4.89 kPa	4

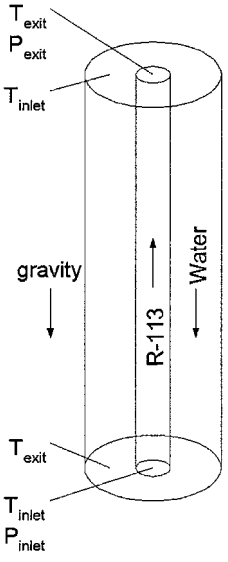

Fig. 1 Test section: annular heat exchanger.

Heat-Transfer Model

Figure 3 illustrates the simple resistance model used to predict heat-transfer characteristics of the system as a function of axial position z. The heat exchanger was divided into 23 (2.54-cm) 1-in. segments. Fluid temperatures (T_{water} and $T_{R\text{-}113}$) and thermodynamic quality were determined at every inch along the test section. Heat addition Q was calculated for each segment using the change in fluid temperature or quality across the segment. Thermal resistance and heat-transfer coefficients were calculated for each segment based on Q. The segment heat-transfer coefficients were then used to predict wall temperatures on the center tube of the heat exchanger. Values of $R_{annulus}$ came from a numerical model created by Lundy[3] for this test facility. R_{wall} was simply the conduction through the center tube wall, and R_{tp} was the two-phase heat-transfer coefficient calculated using this model.

For all of the test data, the water temperature changed less than 2.5°C across the test section. Because this change was small, water

Table 2 Test matrix

Name	Test fluid heater voltage	Test fluid heater power, W	Heating fluid heater voltage	Heating fluid heater power, W
T4H64	4	2	64	266
T9H64	9	11	64	266
T0H74	0	0	74	356
T5H74	5	5	74	356
T11H74	11	11	74	356

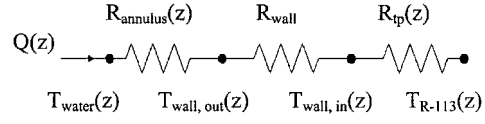

Fig. 3 Resistance heat-transfer model.

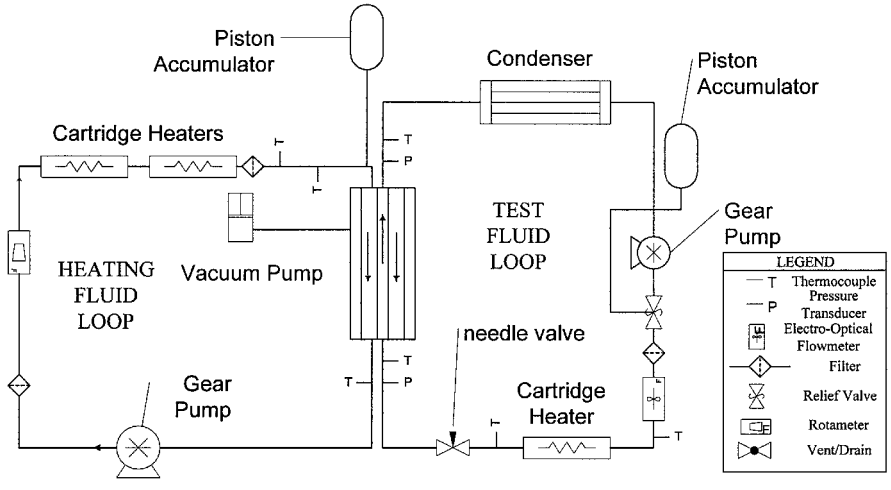

Fig. 2 Experimental apparatus.

Table 3 Flow regime maps

Model	Equations	Major assumptions
Bousman and Dukler[5]	$U_{LS} = \left(\frac{1 - C_0\alpha}{C_0\alpha}\right) U_{GS}$	$C_0 = 1.06$ $\alpha_{B/S} = 0.45$ $\alpha_{S/A} = 0.76$
Balakotaiah et al.[4]	$U_{LS} = \frac{\rho_G}{\rho_L}\frac{\mu_L}{\mu_G}\frac{Su^{\frac{2}{3}}}{K_1} U_{GS}$ $U_{GS} = \frac{K_3 Su^2 \mu_G}{\rho_G D}$	$Su = \rho_L \alpha D/\mu_L^2$ Experimentally determined: $K_1 = 464.16$ $K_3 = 2 \times 10^{-9}$
Barnea[7]	$U_{LS} = \left\{\left[\frac{1 + 75(1-\alpha)}{\alpha^{2.5}}\right](1-\alpha)^2\left(\frac{\mu_G}{\mu_L}\right)^{0.2}\left(\frac{\rho_G}{\rho_L}\right)^{0.8}\right]^{\frac{1}{1.8}} U_{GS}$	$\alpha_{S/A} = 0.76$ Use Bousman and Dukler B/S transition
Baroczy[8]: Earth normal gravity relationship between void fraction and quality	$x = \left\{\left[\frac{(1/\alpha - 1)}{(\rho_G/\rho_L)^{0.65}(\mu_L/\mu_G)^{0.13}}\right]^{\frac{1}{0.74}} + 1\right\}^{-1}$	$\alpha_{B/S} = 0.45$ $\alpha_{S/A} = 0.76$
Slip[1]: using experimental data from Reinarts et al.[3] and this work	$x = \frac{S}{(\rho_L/\rho_G)[(1-\alpha)/\alpha] + S}$	$S_{B/S} = 1.70$ $S_{S/A} = 2.05$ $\alpha_{B/S} = 0.45$ $\alpha_{S/A} = 0.76$

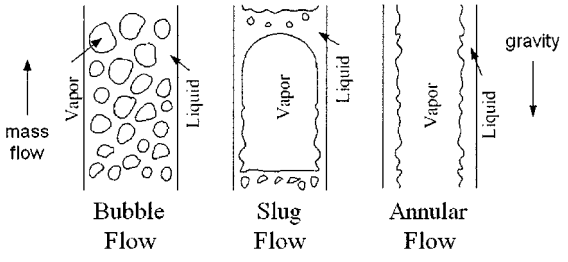

Fig. 4 Typical flow boiling regimes.

temperatures were interpolated linearly between the measured inlet and exit values. The axial temperature profile of the boiling R-113 consisted of two parts. At the entrance of the heat exchanger, the fluid experienced subcooled nucleate boiling. In this portion of the test section, the R-113 temperature was assumed to increase linearly. Once the fluid reached the saturation pressure, the temperature was assumed to be constant as it flowed through the rest of the heat exchanger. The assumption of constant temperature was based on the negligible pressure drop associated with flow boiling in a smooth glass tube and the relationship between pressure and temperature in a two-phase fluid.

The quality was assumed to equal zero while the fluid was subcooled and then increased linearly after the fluid reached a saturated state. The two points required to determine this linear relationship were the qualities at the bubble-to-slug and slug-to-annular flow regime transitions, determined using each of the flow regime maps investigated. Westheimer[1] has performed a more detailed analysis of these assumptions and the heat-transfer model.

Flow Regime Maps

Flow boiling is commonly classified through use of flow boiling regimes. These regimes provide ways to characterize the flow dynamics of the vapor and liquid phases through visual observations. Typical flow regimes for a boiling fluid flowing upward in a vertical tube are shown in Fig. 4. According to Lundy,[3] defining flow regimes is still the topic of debate, even for terrestrial environments. In addition to the bubble, slug, and annular flow regimes shown in Fig. 4, a churn flow regime is often included. Churn flow is usually thought of as a transition from slug to annular flow. Balakotaiah et al.[4] stated that churn flow does not occur in reduced gravity environments. As a result, it was not considered for this work. Another flow regime that should be noted is frothy annular flow. In reduced gravity environments Reinarts et al.[2] observed this frothy annular flow in which vapor bubbles were present in the liquid film of annular flow.

In the following analysis flow regimes were identified to create a linear profile of the R-113 quality axially along the heat exchanger. Because defining flow regimes was not the primary focus of this work, they were simplified to only include bubble, slug, and annular flow. Lundy[3] performed an extensive literature review on flow regime classification and his definitions were adopted for this work: 1) bubble, small dispersed vapor bubbles in a continuous liquid phase; 2) slug, bubble diameter approaches the diameter of the tube and the bubbles take on the characteristic Taylor bubble or bullet shape; and 3) annular, liquid no longer spans the diameter of the tube.

Five flow regime maps were used to relate the transitions between these flow regimes to the quality of the fluid. Most of these models related the superficial velocities of the liquid and vapor phases. These relationships were modified to create equations relating quality and mass flow rate using the definitions listed in the nomenclature section of this paper. Table 3 presents the equations used to predict the transitions from bubble to slug flow and from slug to annular flow used in this work.

Westheimer[1] has provided a more comprehensive explanation of the theories and the assumptions required for each of these models. The assumption of critical void fractions, B/S of 0.45 and S/A of 0.76, at the flow regime transitions was necessary to determine qualities from most of these models. These values are frequently discussed in flow regime literature, including Reinarts et al.,[2] Bousman and Dukler,[5] Chen et al.,[6] and Crowley.[7] These five methods of predicting the quality at flow regime transitions, along with the visual observation at each location were used to create the linear quality profiles in the axial direction of the heat exchanger that enabled this analysis. Figure 5 summarizes the process used to reduce and analyze the data from this experiment.

Results and Discussion

The initial result of this experiment was the collection of extensive visual flow boiling data. The parabolic flights provided an excellent opportunity to see the effect of gravity on the flow boiling process. Figure 6 shows video frames of the experiment during a 1.8-*g* maneuver, and Fig. 7 shows the same portion of the test section a few seconds later while in reduced gravity. These figures show that in a 1.8-*g* environment primarily small bubbles and a chaotic churn flow were found in the test section. Slug flow was almost nonexistent,

probably because of a combination of fluid properties and heating conditions. It also appears that not enough heat was added to the R-113 to achieve annular flow during the 1.8-*g* periods shown here.

Figures 6 and 7 clearly show that by decreasing the gravitational acceleration and maintaining the other test conditions nearly constant the bubbles grew larger and bubble, slug, and annular flow regimes were clearly present. Another observation that these pictures cannot illustrate was that the bubble speed drastically decreased as the test conditions approached reduced gravity. Decreased bubble speed in reduced gravity illustrated the effect of buoyancy on the dynamics of the vapor bubbles. This effect was maximized because of the low R-113 flow rates used in the experiment. Figure 7 illustrates that frothy annular flow was seen in reduced gravity environments. It appears that the frothy annular flow was very similar to churn flow, especially when the trend of larger bubbles in reduced gravity is considered.

Locations along the test section of the flow regime transitions are given in Table 4. These data were used in approximating the quality profile along the test section.

The values in Table 4 are the distances from the bottom of the heat exchanger $z = 0$, where the flow regime transitions were observed to take place. These values represent the average locations for each test condition.

After identifying how changes in gravitational acceleration affected the flow boiling process, the next step was to apply the available analytical tools. The experimental data taken were reduced using the flow regime model of Barnea as presented by Crowley.[7] Figure 8 shows these data on a flow regime map plotted using superficial velocities. The flow regime transitions of Barnea are shown as the solid lines, while the dotted lines in Fig. 8 are a terrestrial flow regime map by McQuillen and Whalley.[8] Lundy[1] previously used the McQuillen and Whalley flow regime map to analyze data from this experimental facility at Earth normal gravity with reasonable success.

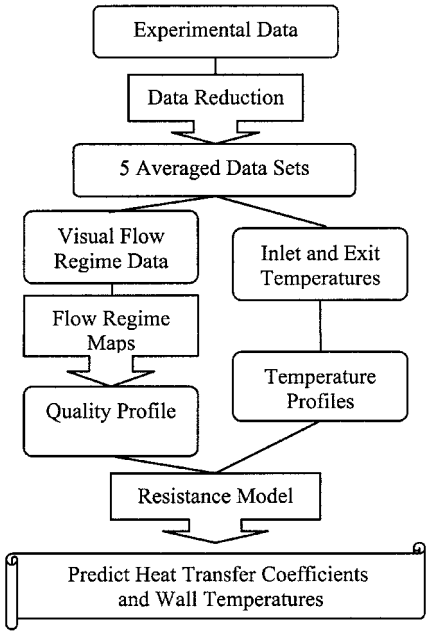

Fig. 5 Analysis flowchart.

Table 4 Flow regime transition locations

Name	Bubble/slug, mm (in.)	Slug/annular mm (in.)
T4H64	237 (9.33)	457 (18)
T9H64	218 (8.6)	432 (17)
T0H74	140 (5.5)	280 (11)
T5H74	135 (5.33)	280 (11)
T11H74	140 (5.5)	280 (11)

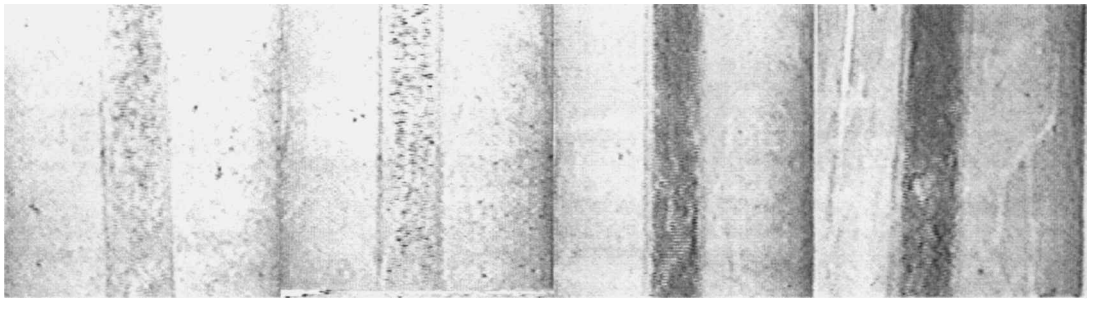

Fig. 6 Visual data, 1.8 *g*.

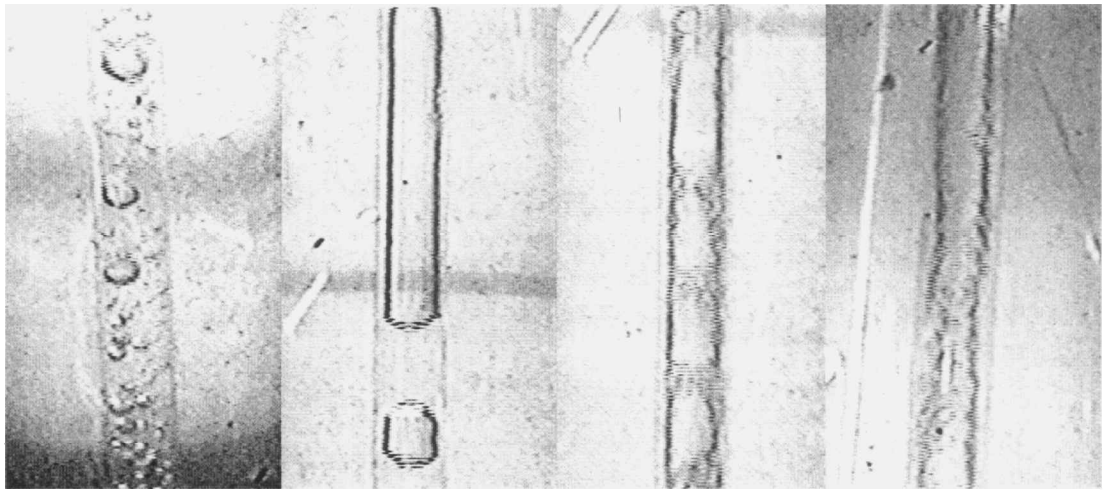

Fig. 7 Visual data, 0 *g*.

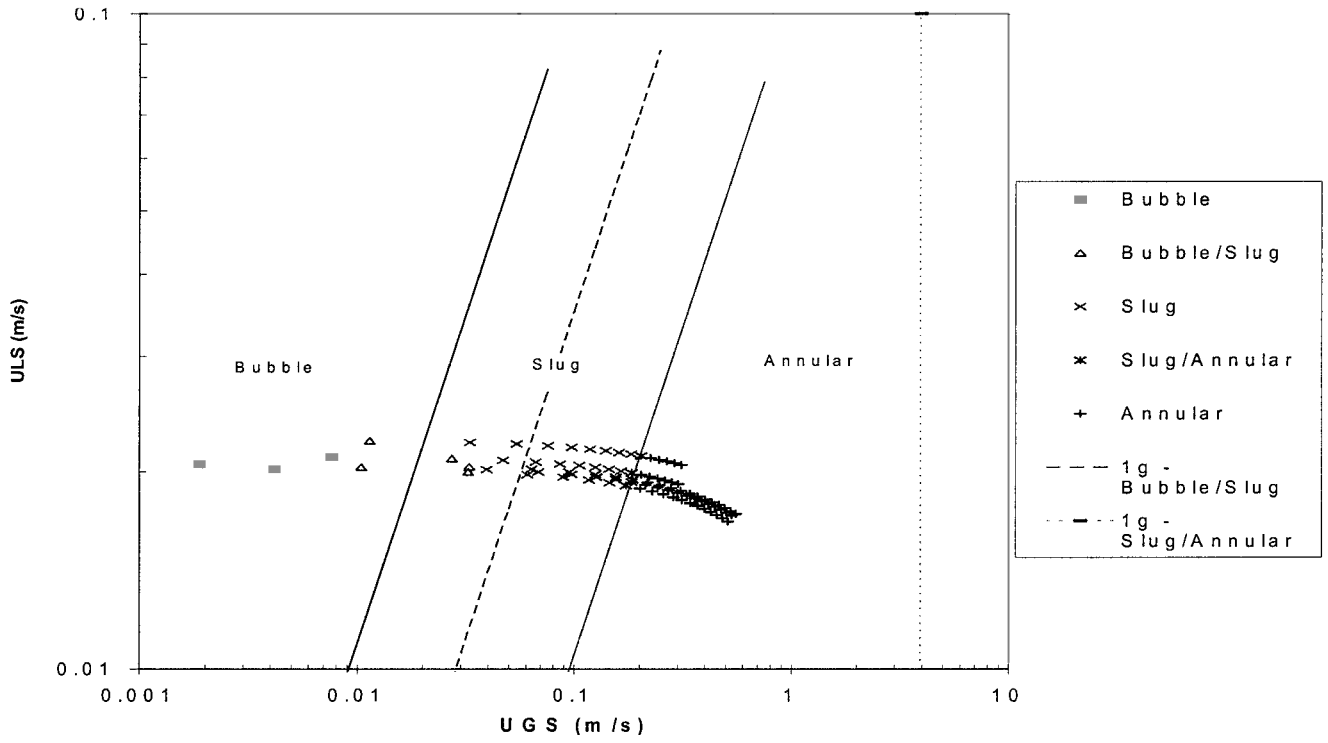

Fig. 8 Superficial velocity flow regime map, Barnea 0-*g* correlation.

Not surprisingly, the reduced gravity data corresponded quite well with the reduced gravity map of Barnea. This was because the flow regime transitions were used to reduce the data. However, the 1-*g* correlations did not agree well with the reduced gravity data. These flow regime maps predict that reduced gravity flow regime transitions occurred at lower superficial vapor velocities than their normal gravity counterparts. This shift in flow regime transitions was clearly seen in the visual data. For example, bubble flow in 1.8-*g* changed to slug flow as the acceleration decreased, because gravity was reduced.

The slug to annular transition was harder to compare because of the presence of churn and frothy annular flow. To simplify, annular flow was observed during 0-*g* periods of the visual data, but was not observed during 1.8-*g* periods at the same test settings. This observation, in combination with Fig. 8, suggested that the superficial vapor velocities were not high enough to create annular flow in the 1.8-*g* environment.

Figure 9 shows the microgravity map of Barnea and the 1-*g* flow regime map of McQuillen and Whalley[8] with quality given as a function of mass flow rate. This graph exhibits the same shift as Fig. 8, except instead of the superficial vapor velocity the quality at the flow regime transitions decreased with decreasing gravitational acceleration. The transition from slug to annular flow predicted using the 1-*g* flow regime map corresponded to a quality approaching unity and was not shown on Fig. 9.

Comparing qualities at the flow regime transitions provided an easy thermodynamic comparison between flow boiling in reduced and normal gravity environments. Because the quality was lower in reduced gravity, less heat addition was needed to reach these flow regime transitions.

By applying these flow regime maps, it was possible to make predictions of the heat-transfer coefficient and tube wall temperatures as a function of axial position along the heat exchanger. Figures 10 and 11 illustrate these profiles for the T4H64 test point. Figure 10 shows the quality profile x created using visual observations of the locations of flow regime transitions and the Barnea model, as well as the heat-transfer coefficient in the annulus U_{annulus} of the heat exchanger and the calculation of the two-phase heat-transfer coefficient of the R-113. Each of the test points produced a similar graph where the two-phase heat-transfer coefficient increased from

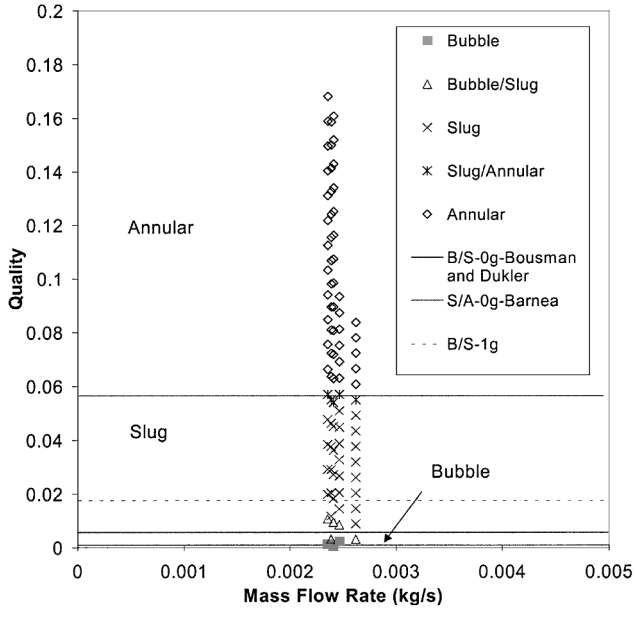

Fig. 9 Quality vs mass flow rate flow regime map, Barnea 0-*g* correlation.

the entrance of the heat exchanger, peaked near the point where the fluid reached the saturated state, and then decreased to the exit. Peak heat-transfer coefficients and the initial point of saturation also corresponded to the bubble to slug flow regime transition. All of the curves in Figs. 10 and 11 shifted to the left for test points with larger applied heat loads.

Large uncertainties were associated with the actual value of the peak, or maximum heat-transfer coefficient, because of numerical uncertainties of the resistance model. These uncertainties accumulated from the conduction coefficient of the glass tube, the heat-transfer coefficient in the annulus of the heat exchanger, and the assumptions of the R-113 temperature and quality profiles. Two-phase heat-transfer coefficients and tube wall temperatures were

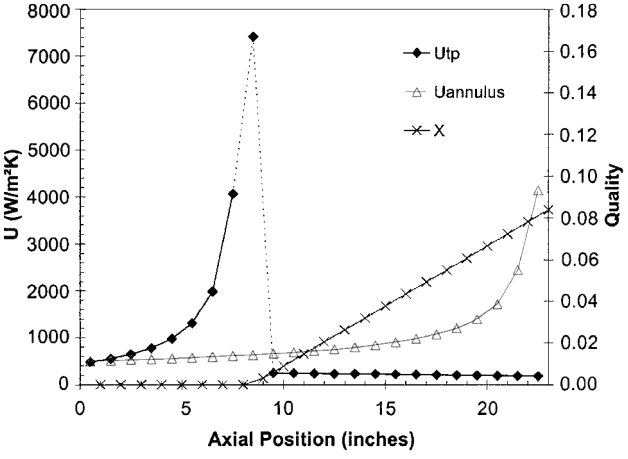

Fig. 10 Heat-transfer coefficient profile, T4H64.

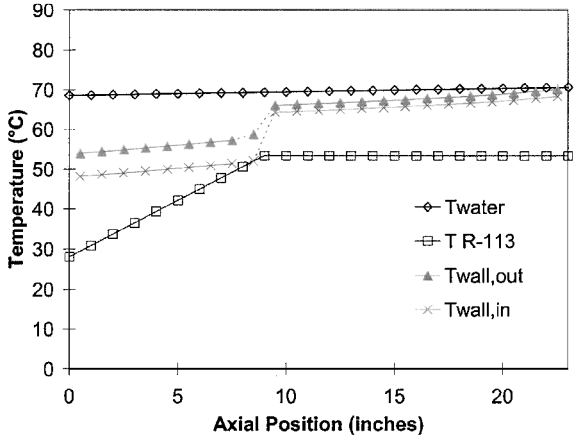

Fig. 11 Wall temperature profile, T4H64.

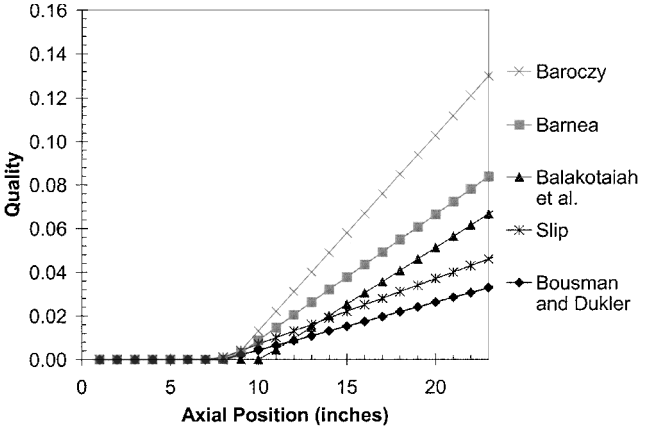

Fig. 12 Axial quality profile, flow regime model comparison.

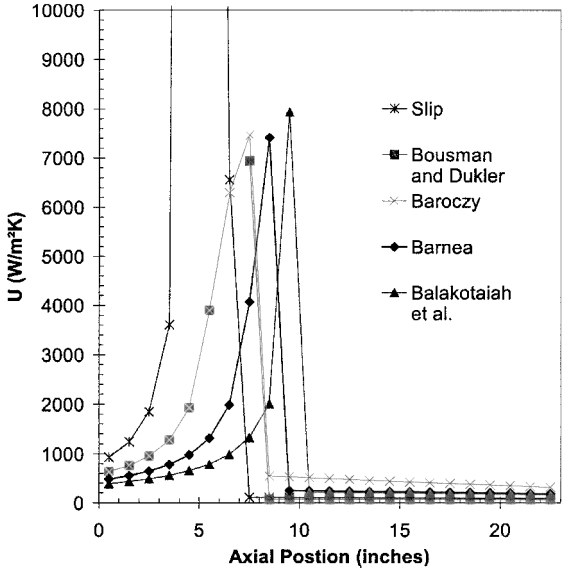

Fig. 13 Axial heat-transfer coefficient profiles, flow regime model comparison.

approximated near the peak locations because of this error. Regions where these values are approximated were shown on the figures as dotted lines. Westheimer[1] gives a more detailed explanation of how these approximations were developed.

These heat-transfer coefficient profiles agree with the previous work of Carey,[9] who explained that the maximum heat transfer coefficient for flow boiling in a tube corresponds with the maximum nucleate boiling. Nucleate boiling is dominant in bubble and at the beginning of slug flow. Carey also explained that as annular flow is approached the nucleate boiling is suppressed and the two-phase heat-transfer coefficient decreases. Although this model was not actually based on these heat-transfer mechanisms, the fact that the heat-transfer coefficient prediction and visual flow regime observations agree with Carey's assessment indicates that the assumptions made in the model are reasonable.

Figure 11 shows the temperature profile calculated using the resistance model. T_{water}, $T_{R\text{-}113}$, $T_{wall\ out}$, and $T_{wall\ in}$ represent the temperatures of the water R-113, outside of the center tube wall and inside of the center tube wall, respectively. The temperature on the inner wall of the tube approaches the temperature of the R-113 at the axial location corresponding to the maximum two-phase heat-transfer coefficient.

Finally the effects of the different flow regime models on the quality and two-phase heat-transfer coefficient profiles were examined. Figure 12 illustrates quality profiles produced by all five flow regime models for the T4H64 test condition. The two key characteristics noted were the location where the fluid becomes saturated and the slope of the linear profile.

The initial saturation point varied about 2 in. (50 mm). The slip model predicted the location nearest to the inlet, whereas the Balakotaiah et al. model[4] predicted the point farthest from the inlet of the heat exchanger. Exit qualities ranged from 0.035 to 0.139. The Bousman and Dukler model predicted the lowest value, and the Baroczy equation predicted the highest one.

Figure 13 shows the two-phase heat-transfer coefficient profiles calculated using the different flow regime models. The major observation taken from this graph was that the maximum heat-transfer coefficient shifted according to the location where the fluid became saturated. Similar to Fig. 12, the peak using the slip model was closest to the inlet of the heat exchanger, whereas the Balakotaiah et al. model predicted the location farthest away. The axial positions of these peaks ranged from 5.5 to 9.5 in. (140 to 241 mm) along the test section. It is again noted that the actual value of the maximum two-phase heat transfer coefficient was greatly affected by inaccuracies in the resistance model. The slip model and the Bousman and Dukler flow regime map predicted peak values of the two-phase heat-transfer coefficient that were too large to effectively show on this graph.[10]

Conclusions

As expected, the results of this investigation indicated that the fluid dynamics of flow boiling are strongly gravity dependent. This was clearly apparent in the visual data and in the shift of the flow regime maps. Less heat addition was necessary in reduced gravity for the flow regime transitions to occur. This gravity dependence requires that engineers use caution when designing two-phase systems for use in environments of different gravitational accelerations. Crowley and Izenson[10] make a similar statement in their *Design Manual for Microgravity Two-Phase Flow and Heat Transfer.*

Comparing results from the test conditions illustrated two trends. Increasing the heater setting resulted in the flow regime transitions taking place closer to the inlet of the heat exchanger. This also moved the peak of the heat-transfer coefficient profile closer to the inlet.

Crowley and Izenson[10] suggest that gravity affects the bubble and slug flow regimes most greatly and recommend that two-phase systems intended for use in different gravitational environments be designed to avoid these flow regimes. In contradiction, the results from this study indicate that the highest heat-transfer coefficients occur in these flow regimes because of maximized nucleate boiling. This suggests that more work should be performed in order to optimize the design of two-phase heat-transfer equipment in reduced gravity.

Large differences in visual data and analysis demonstrated that Earth-based flow regime maps poorly represent reduced gravity behavior. However, all of the reduced gravity flow regime maps produced similar results for heat-transfer coefficient and wall temperature calculations. Therefore any of the 0-*g* flow regime maps would have been acceptable for the analysis presented in this work.

In summary, this investigation succeeded in adding new and unique data to the two-phase flow reduced gravity database. It also demonstrated both the potential for excellent heat-transfer enhancement during nucleate boiling and for the use of two-phase thermal systems in space applications.[10]

Acknowledgments

Support for this research was provided by NASA's Office of Life and Microgravity Sciences and Applications, the Texas Space Grant Consortium, and the National Science Foundation. B. Motil's assistance in bringing the experiment to flight readiness, along with J. Yaniec and J. Rickard's help during the actual flights are greatly appreciated.

References

[1]Westheimer, D., "A Visualization Study of Flow Dynamics and Heat Transfer in Reduced Gravity Flow Boiling," M. S. Thesis, Dept. of Mechanical Engineering, Texas A&M Univ., College Station, TX, May 2000.

[2]Reinarts, T. R., Miller, K. M., and Best, F. R., "Two-Phase Flow Regimes in Smooth Tubing in Microgravity, Lunar Gravity, Martian Gravity, and Earth-Normal Gravity," *Proceedings of the 1993 ASME Winter Annual Meeting, Fluid Mechanics Phenomena in Microgravity 1993*, American Society of Mechanical Engineers, New York, 1993, pp. 85–103.

[3]Lundy, B. F., "A Visualization Comparison of Convective Flow Boiling Heat Transfer Augmentation Devices," M. S. Thesis, Dept. of Mechanical Engineering, Texas A&M Univ., College Station, TX, Dec. 1998.

[4]Balakotaiah, V., Jayawardena, S. S., and Nguyen, L. T., "Studies on Normal and Microgravity Annular Two Phase Flows," *Proceedings of the Fourth Microgravity Fluid Physics & Transport Phenomena Conference*, NASA Office of Life and Microgravity Science & Applications, Cleveland, OH, 1998, pp. 6–12.

[5]Bousman, W. S., and Dukler, A. E., "Studies of Gas-Liquid Flow in Microgravity: Void Fraction, Pressure Drop and Flow Patterns," *Proceedings of the 1993 ASME Winter Annual Meeting, Fluid Mechanics Phenomena in Microgravity 1993*, American Society of Mechanical Engineers, New York, 1993, pp. 23–36.

[6]Chen, I. Y., Downing, R., Keshock, E. G., and Al-Sharif, M., "Measurements and Correlation of Two-Phase Pressure Drop Under Microgravity Conditions," *Journal of Thermophysics and Heat Transfer*, Vol. 5, No. 4, 1991, pp. 414–423.

[7]Crowley, C. J., "Unified Flow Regime Predictions at Earth Gravity and Microgravity," *Heat Transfer in Space Systems*, American Society of Mechanical Engineers, New York, 1990, pp. 63–75.

[8]McQuillan, K. W., and Whalley, P. B., "Flow Patterns in Vertical Two-Phase Flow," *International Journal of Multiphase Flow*, Vol. 11, No. 2, 1985, pp. 161–175.

[9]Carey, V. P., *Liquid-Vapor Phase-Change Phenomena*, Taylor and Francis, Washington, DC, 1992, pp. 167–186.

[10]Crowley, C. J., and Izenson, M. G., *Design Manual for Microgravity Two-Phase Flow and Heat Transfer,* Creare Inc., Rept. A-1463, Hanover, NH, Oct. 1989.